Silver nanoparticles/free-standing carbon nanotubes Janus membranes.

D. Ibañez[a,1,]*, M. Galindo[a,b], A. Colina[a,1], E. Valles[b,1], A. Heras[a,1], E. Gomez[b,1,]*

a. Department of Chemistry, Universidad de Burgos, Pza. Misael Bañuelos s/n, E-09001 Burgos, Spain.

b. Grup d'Electrodeposició de Capes Primes i Nanoestructures (GE-CPN). Dep. Ciència de Materials i Química Física and Institut de Nanociència i Nanotecnologia (IN2UB). Universitat de Barcelona, 08028 Barcelona, Spain.

* Corresponding author: dibanez@ubu.es; e.gomez@ub.edu

1. ISE member.

Abstract

Janus materials are attracting intense interest due to their exceptional possibilities in the design of structures with specific properties. In this work, Janus structures were constructed by the functionalization of free-standing single-walled carbon nanotubes (FS-SWCNT) membranes with silver nanoparticles (AgNPs) electrodeposited on one face of the free-standing structure. The modification of the FS-SWCNT films with AgNPs was carried out from an ionic liquid solution, a green and environmentally friendly procedure. Before the functionalization of the free-standing membranes, the optimal electrodeposition conditions of AgNPs from an ionic liquid in different carbon substrates were studied. We demonstrate by UV-Vis spectroelectrochemistry that the functionalization of the FS-SWCNT membranes on only one face is achieved, remaining unmodified the other face, as SEM images confirm. Moreover, the morphology of AgNPs, and, consequently, the properties of the Janus structures strongly depend on the specific electrodeposition conditions selected, determining their future applicability.

Keywords: Janus materials; free-standing electrodes; silver nanoparticles; ionic liquids; spectroelectrochemistry.

1. Introduction

Janus materials are a new generation of nanomaterials that open a wide field of possibilities in materials chemistry since the biased functionalization of a nanomaterial allows tuning or enhancing some of their properties. For instance, Janus materials can be provided with one hydrophilic side while the other one has hydrophobic properties, or with an area negatively charged and another positively charged, or with different catalytic, optical and/or magnetic

properties in each of their faces [1–4]. The design of materials with specific properties has led to a whole branch of applications for Janus structures in multitude fields, such as in the upgrade of new and more powerful sensors, in electronics, in catalysis, or in the development of new medical devices to facilitate the control of drug delivery [5–7]. Many materials are employed in the fabrication of Janus structures. Here, carbon nanotubes (CNT) have been selected as base material to generate Janus structures due to their widely known advantages as electrical conductor with respect to other classic electrode materials [8–11]. In particular, it should be noted that in this work an innovative factor is proposed to fabricate Janus structures based on carbon nanotubes, like is the use of free-standing single-walled carbon nanotubes (FS-SWCNT). The use of these thin carbon nanotubes membranes as electrodes and their modification with different nanomaterials on each side open the door to an infinite number of applications, such as electrochemical sensors, laser absorber, gas flowmeter, gas heater, supercapacitors, in thermoacoustic applications and in batteries [12–17]. The exceptional mechanic, electric, electronic and thermal properties of SWCNTs make them one of the most fascinating substrates for the fabrication of Janus membranes.

Although different methods can be followed to develop Janus structures [6,7,18,19], our interest is focused on the electrochemical functionalization because this procedure has been proven to be one of the least expensive and more productive for this purpose, allowing the preparation of a wide range of nanostructures. Silver nanostructures are widely used in many fields such as antibacterial agent, catalyst for variety of reactions, modifier of electrodes for improving conductivity, or substrate for surface-enhanced Raman scattering (SERS) applications [20–24]. There is a substantial literature on the electrochemical preparation of silver structures in aqueous medium [25–35], highly dependent on the bath's composition and on the

electrodeposition conditions as the manner that different morphologies and structures could be obtained. However, more recently, different deep eutectic solvents [36–38], chloroaluminate melts [39,40] and room-temperature ionic liquids [41–49] are receiving a growing attention as green electroplating solutions for silver deposition taking advantage of thermal and chemical stability, negligible low vapour pressure, reasonable ionic conductivity and moderate viscosity of these new solvent. Due to the high positive standard potential value of silver and with the aim of tailoring the silver deposition at less positive potentials than in aqueous medium without the use of extreme low concentrations we explore the AgNPs deposition in ionic liquids. The good solubility of silver compounds in these media, makes them attractive and alternative solvents for environmentally friendly processes. The ionic liquid selected has been 1-butyl-1-methylpyrrolidinium bis(trifluoromethanesulfonyl)imide (BmpyrNTf$_2$) that is an air and water stable liquid, immiscible in water showing hydrophobic behavior. The selection of this ionic liquid was performed attending to its immiscibility in water, because in this way, it avoids the diffusion along the electrode, as well as the ability to be easily handled in the atmosphere. Although silver electrodeposition has been already reported in this ionic liquid [44], to assess the feasibility of obtaining AgNPs on FS-SWCNTs membranes, the effect of lowering the analytical Ag(I) concentration and the influence of the electrodeposition substrate must be analyzed.

Furthermore, the good transparency to UV-Vis radiation and the suitable conductivity demonstrated by the FS-SWCNT electrodes [50], allow us to study diverse processes that take place on the electrode surface by UV-Vis absorption spectroelectrochemistry. Spectroelectrochemistry is one of the most powerful techniques in the study of a huge variety of chemical systems [51–53]. The combination of electrochemistry and spectroscopy is undoubtedly a successful coupling; it provides simultaneously the advantages of both techniques

and offers very unique possibilities that are not achievable by electrochemistry or spectroscopy independently. The great usefulness of this technique has been reflected in the study of, for example, reaction mechanisms, compounds of biological interest, characterization of compounds and materials of completely different nature, diffusive and adsorptive processes, and quantitative analysis [51,54–57].

Therefore, the main objective of this work is to obtain a Janus nanostructure by functionalization of only one face of a FS-SWCNT membrane by the electrodeposition of AgNPs from an ionic liquid solution. In this way, a hybrid nanomaterial is obtained with the characteristic properties of SWCNTs on one face, and those specific of AgNPs on the other.

2. Material and methods

2.1. Reagents

Chemicals used were silver nitrate ($AgNO_3$, Panreac), and 1-butyl-1-methylpyrrolidinium bis(trifluoromethanesulfonyl)imide ($BmpyrNTf_2$, Solvionic), all of them of analytical grade. The ionic solvent was liquid at room temperature and non-miscible in water. The kinematic viscosity of $BmpyrNTf_2$ at 20 ºC is 548 St (kinematic viscosity of water at 20 ºC = 0.01 St) and its conductivity is 2.68 mS cm^{-1} at 20°C and 2.94 mS cm^{-1} at 25°C.

SWCNT (Sigma-Aldrich) dispersion was prepared using 1,2-dichloroethane (DCE, Acros Organics) as solvent. SWCNT electrodes were fabricated using hydrophilic polytetrafluoroethylene (PTFE) filters (pore size 0.1 μm, JVWP01300, Millipore Omnipore). Free-standing SWCNT electrodes (FS-SWCNT) were prepared using nitrocellulose filters (pore size of 0.45 μm, HAWP01300, Millipore Omnipore) and acetone (VWR). Both SWCNT and FS-SWCNT electrodes were fabricated using poly(ethylene terephthalate) (PET, 175 mm thick, HiFi

Industrial Film) as physical support, conductive silver paint (Electrolube) for ohmic contacts and Kapton® as high temp masking tape (RS Components).

For safety considerations, all handling and processing were performed carefully, particularly when DCE was used.

2.2. Fabrication of SWCNT and FS-SWCNT electrodes.

The fabrication of SWCNT and FS-SWCNT electrodes (Fig. S1 in Supporting Information), used as working electrodes, was carried out base on the methodology described in previous works [50,58,59]. SWCNT solution used for preparing both SWCNT and FS-SWCNT electrodes was dispersed using a CY-500 tip-sonicator (Optic ivymen System).

The SWCNT electrodes were prepared by filtering 0.8 mL of a sonicated SWCNT homogeneous dispersion in DCE (5 mg/L) through a PTFE filter. The filter with the SWCNT film was dried at room temperature for five minutes to achieve a proper transference during the next step. The press-transference of the SWCNT film to the PET sheets was performed by applying 27 ± 2 tons for about one minute using a hydraulic press. Finally, the PTFE filter was carefully peeled off using tweezers while the SWCNT film remains attached to the PET sheet (Fig. S1a in Supporting Information).

The methodology employed for the fabrication of the FS-SWCNT electrodes involves the filtration under vacuum of 3 mL of the same SWCNT dispersion in DCE than in the previous case but using a nitrocellulose filter instead of a PTFE filter. The homogeneous SWCNT film was immediately low-pressure transferred on the PET sheet applying only a slight finger pressure. In this case, the PET sheet has a hole of 2 mm in diameter (Fig. S1c in Supporting Information). SWCNT film is carefully and thoroughly rinsed with acetone for 15 min to achieve

the complete removal of the filter without breaking the FS-SWCNT film (Fig. S1b in Supporting Information).

The final step is identical for the two types of electrodes; after the SWCNT film is dried at room temperature, the ohmic contact is made using a conductive silver paint. The silver paint is dried in an oven at 75 °C for 30 min, and allowed to cool before coating the contact using a high temp masking tape (Kapton).

2.3. Instrumentation

All electrochemical measurements were carried out using a potentiostat AUTOLAB PGSTAT 12 electrochemical system. The basic electrochemical study was performed using a glassy carbon electrode (GC, Metrohm) as working electrode, polished to a mirror finish using alumina powder of different grades (3.75 and 1.87 μm VWR Prolabo), cleaned ultrasonically for 2 min in high-quality water (resistivity of 18.2 MΩ cm, MilliQ gradient A10 system, Millipore) and dried with air prior to be immersed in the solution.

Counter and reference electrodes were a spiral of platinum and a homemade Ag/AgCl/KCl (3M), respectively. Stable and reproducible values of the potential were obtained using these homemade reference electrodes.

Voltammetric experiments were carried out at 0.010 V s^{-1}, scanning first the potential to negative values. Chronoamperometric experiments were performed starting from a potential where no process took place to the selected potential value. Electrochemical reproducibility was getting hard and laborious at room temperature due to the lower conductivity of the ionic liquids. In the optimization process of electrodeposition of AgNPs, when GC or SWCNT electrodes were used, the working temperature was kept constant at 70 ºC to favour low viscosity and high

conductivity of the solution. All electrochemical experiments were carried out using these experimental conditions unless different ones were specified.

Morphology was observed using a scanning electron microscope Field Emission JSM-7100F Analytical Microscopy.

UV−Vis absorption spectroelectrochemistry measurements in normal transmission configuration were performed using a QE65000 spectrometer (Ocean Optics) coupled and synchronized with the potentiostat. The light beam, supplied by a light source (AvaLight-DH-S-BAL, Avantes), was conducted to the spectroelectrochemical cell by a 230 μm optical fiber (Ocean Optics) and collected from the spectroelectrochemical cell and led it to the spectrometer by a 200 μm optical fiber probe (Avantes).

3. Results and Discussion

In order to optimize the electrochemical reduction conditions of Ag(I) in BmpyrNTf$_2$, different carbon substrates were used as working electrodes: GC, SWCNT and FS-SWCNT.

3.1. Silver electrodeposition on GC electrodes

Ag electrodeposition and its redissolution on GC were studied by cyclic voltammetry, scanning the potential from +1.00 V to -0.95 V and back to +1.00 V in 8×10^{-3} M AgNO$_3$ in BmpyrNTf$_2$. Voltammetric profile (red line in Fig. 1a) shows in the cathodic scan a sharp current increase that develops in a well-defined reduction peak (C$_1$) at +0.47 V, after which the current increases smoothly. Lengthening the cathodic scan to more negative values another reduction peak (C$_2$) at -0.33 V is observed, previous to the massive reduction of the ionic liquid at potentials lower than -0.85 V (blank experiment performed only in BmpyrNTf$_2$, blue line in Fig.

1a). In the positive scan a single anodic peak (A_1) at +0.77 V related to the Ag oxidation was observed.

Electrochemistry was also carried out scanning the potential in a shorter potential window, from +0.90 V to -0.10 V and back to +0.90 V, to study if both cathodic peaks, C_1 and C_2, were related to the reduction of Ag(I). Cyclic voltammogram (CV), Fig. S2 in Supporting Information, demonstrates that when the second reduction process (C_2) does not occur the involved charge in the oxidation peak A_1 does not show relevant changes. Therefore the C_2 reduction peak seems to be associated with other process different to the reduction of Ag(I). To establish the origin of the C_2 reduction peak, a CV of a blank solution with only the ionic liquid using a GC was carried out. The electrochemical response of the $BmpyrNTf_2$ (purple line in Fig. 1b) does not show reduction peaks and only a shoulder previous to massive reduction of the ionic liquid is observed. A new voltammetric study (green line in Fig. 1b) was performed in the blank solution, but in this case, using a small Ag ball as a working electrode instead of the GC substrate. As can be observed, in the negative scan a new current peak previous to the massive current related to the reduction of the ionic liquid was recorded. These results seem to confirm that this new reduction peak can be associated with the presence of metallic Ag. Additionally, it can be seen that using the Ag ball working electrode the cathodic current related to the solvent reduction was advanced 0.22 V respect to the GC electrode. Similar advancement of the onset of the current was previously detected over other metallic substrates [37]. Therefore, it suggests that the presence of Ag modifies the reduction process of the solvent in the way that the ionic liquid can be reduced both on the carbon substrate and on the Ag electrodeposited. Thus, the detected C_2 peak from the Ag(I) solution (red line in Fig. 1a) is mainly related to solvent reduction process on the Ag freshly deposited on the GC electrode.

Different potentiostatic experiments were performed to study the Ag electrodeposition on the GC electrode from the BmpyrNTf$_2$ ionic liquid. From the Ag(I) solution, the potentiostatic curves were recorded after applying a single potential step, from a potential at which no process occurs to potential values at which Ag reduction took place. The potential range selected for these experiments was the corresponding to the decreasing part of the voltammetric C$_1$ peak (red line in Fig. 1a). All current transients (Fig. 2) exhibit the typical profile for nucleation and three dimensional growth, i.e., a current rising part that attains a maximum from which the current decays with increasing time. Comparison of the curves obtained at different potentials evidences that the current density corresponding to the maximum (j$_m$) is greater as the overpotential increases, being the corresponding time at which the maximum appears (t$_m$) shortened (Fig. 2). For all potentials, the descending part of the transients tends to overlap. This behavior corresponds to a process controlled by mass transfer of the electroactive species towards the electrode. The initial stage of nucleation and crystal growth of Ag electrodeposited on GC was analyzed. In order to establish the nucleation mechanism at the different potentials, j-t transients recorded in Fig. 2 were compared in Fig. S3 in Supporting Information with the theoretical model provided by Scharifker and Hills [60,61], devoted to processes in which mass control is the limiting step. This model proposes that, in dimensionless form, instantaneous nucleation (all nuclei immediately formed after the step potential) and progressive nucleation (nuclei formed according to kinetics) follow the equations:

$$\left(\frac{j}{j_{max}}\right)^2 = 1.9542\left(\frac{t}{t_m}\right)^{-1}\left[1-\exp\left(-1.2564\frac{t}{t_m}\right)\right]^2 \tag{1}$$

for instantaneous nucleation, and:

$$\left(\frac{j}{j_{max}}\right)^2 = 1.2254\left(\frac{t}{t_m}\right)^{-1}\left[1-\exp\left(-2.3367\left(\frac{t}{t_m}\right)^2\right)\right]^2 \qquad (2)$$

for progressive nucleation.

Comparison of the non-dimensional plots with the corresponding to limit situations of instantaneous and progressive nucleation (blue and red lines in Fig. S3 in Supporting Information) shows that, in the experiments included in Fig. 2, Ag nuclei were formed quasi instantaneously. These results agree with previous work [44] at lower temperature. It is well established that in aqueous media Ag deposition occurs easily, as the manner that the deposition process occurs at very low overpotentials [62], whereas when Ag(I) is complexed the electrodeposition takes place at more negative potentials [37]. Even under these conditions, moderate overpotentials are sufficient to attain instantaneous nucleation.

In order to analyze the role of the applied potential over the growth of Ag electrodeposits, a morphological analysis was performed for samples prepared at fixed charge (8 mC). With this objective, potentials belonging at different regions were selected taking as reference the CV of Fig. 1a: (1) +0.56 V that corresponds to the current increase of peak C_1, (2) +0.16 V, potential between the two cathodic peaks, and (3) -0.60 V, potential after the second cathodic peak C_2. Fig. 3a shows that Ag electrodeposition at the low overpotential, +0.56 V, begins by isolated grains and the increase of the deposition charge causes the formation of blocks of different size, in the micrometric order. Increasing the overpotential, +0.16 V, the deposit obtained (Fig. 3b) exhibits also a grained morphology in which the grain size is reduced, and at this relative high charge the deposit is formed by piled up grains. Finally, the third sample was prepared in the potential range corresponding to the onset of the reduction peak C_2. SEM image (Fig. 3c) indicates that less defined grains are formed and that the 3D growth are more inhibited respect to

that observed in the two previous cases. By comparison of the SEM image at -0.60 V with those of the samples prepared at more positive potentials (Fig. 3a and 3b), the Ag deposit seems to correspond to a process in which the deposition charge involved is lower than the one actually applied. As can be noticed, flat grains around 100 nm were obtained. This morphology could be related to the simultaneous reduction of Ag(I) and the ionic liquid that seems to be favoured, in this potential range, by the presence of Ag previously deposited. Therefore, it can be concluded that the charge passed was involved in the co-reduction of the solvent and the Ag(I).

These results confirm the Ag electrodeposition from BmpyrNTf$_2$ solvent on GC at this low concentration and, furthermore, this overview about the deposition process will be useful to test this solution in the functionalization of other carbon materials by AgNPs. Moreover, under these experimental conditions no coalescence was achieved, making the Ag(I) in BmpyrNTf$_2$ solution eligible to functionalize carbon nanomaterials, such as SWCNTs, with AgNPs.

3.2. AgNPs electrodeposition on SWCNT electrodes

The electrodeposition of AgNPs on SWCNT electrodes (Fig. S1a in Supporting Information) was performed as the second step of this work, previous step to the functionalization of FS-SWCNT electrodes, to test and compare the electrochemical behaviour and the morphology of the AgNPs obtained using another kind of carbon substrate. Cyclic voltammetry was carried out in BmpyrNTf$_2$, scanning the potential from +1.20 V to -0.70 V and back to +1.20 V. Fig. S4 in Supporting Information displays the CV obtained on a SWCNT electrode for the reduction of Ag(I) to Ag(0) and its redissolution. Voltammetric experiments performed using the SWCNT electrodes, prepared according to the conditions specified in the experimental section, revealed that the electrochemical behavior was similar to the voltammetric response observed previously

on GC: cathodic scan shows two reduction peaks prior the massive ionic solvent reduction, and the anodic scan displays a unique oxidation peak related to the silver oxidation. The onset potential of the deposition current related to C_1 process was delayed 0.25 V respect to the observed on GC substrate. It is remarkable that the relationship between the two reduction processes, C_1 and C_2, j_{C1}/j_{C2} is 13 times higher when a SWCNT electrode is selected as working electrode than when a GC is used. Comparison between the current density of the voltammetric peaks, C_1 and C_2, suggests that the increase of j_{C1}/j_{C2} observed is due to the nature of the SWCNT electrode prepared, the initio of deposition is delayed, but once started the reduction of Ag(I) proceeds and accordingly, the value of j_{C1} is higher. Consecutive scans lead to a substantial increase of the involved charge under the C_2 reduction peak, being the relationship between the two reduction processes j_{C1}/j_{C2} 10.5 times lower in the third scan than in the first one. As was established in the Section 3.1, C_2 reduction peak is associated with the presence of metallic Ag, thus the decrease of j_{C1}/j_{C2} in the third scan is related to the increase of the amount of metallic Ag deposited on the SWCNT electrode with the number of potential cycles.

Attending to the previous results on GC, different AgNPs samples were prepared potentiostatically. Taking into account the results obtained with GC in section 3.1 and that our final interest is the deposition of AgNPs with a narrow distribution of size, lower potentials than the C_1 peak, peaking at +0.30 V, and higher than C_2 peak were selected. This range of potentials, from +0.20 V to -0.10 V, favours the instantaneous nucleation and it avoids the range of potentials at which ionic liquid solvent reduction takes place. The experimental conditions selected for all samples lead to potentiostatic transients with similar profile respect to the observed in Fig. S5 in Supporting Information, in which the maximum appears at extremely low deposition times.

Uniformity and size of the AgNPs electrogenerated by fixing a deposition charge and applying different reduction potentials, were studied by SEM images. Fig. 4a and 4b show the SEM images of two samples prepared on a SWCNT electrode applying +0.05 V and 0.00 V, respectively, demonstrating the viability of SWCNT electrodes for the electrodeposition of AgNPs from the selected ionic liquid solution. The AgNPs generated were quasi-spherical, without structuration, related to the low charge involved in the electrodeposition process respect to the SWCNT electrode area. These AgNPs showed higher polydispersity at lower overpotentials (Fig. 4a) indicating that although the shape of the corresponding transient corresponds to fast deposition, instantaneous nucleation was not achieved. The medium size at the higher overpotential (Fig. 4b) was around 66 ± 7 nm, experimental conditions where a clear tendency to homogenization of particle size was appreciated. As can be noticed in Fig. 4, the electrodeposition of AgNPs under these experimental conditions does not show specific distribution, and AgNPs are located on the entire surface of the SWCNT film.

To confirm the inconvenience of the preparation of AgNPs in the potential range corresponding to the C_2 peak, some experiments were performed applying potentials around this second reduction peak. Fig. S6 in Supporting Information displays the SEM image of the AgNPs obtained applying a potential of -0.45 V. As can be noticed, a low amount of polydisperse NPs was electrodeposited on the SWCNT electrode. This result confirms that at these overpotentials the deposition charge was used to, at least, two processes, the reduction of Ag(I) to AgNPs and the reduction of the ionic liquid, as was proposed in section 3.1 in GC electrodes.

To achieve the electrosynthesis of smaller AgNPs, the effect of decrease the deposition charge involved in the process was analyzed, maintaining constant the electroactive area and other experimental conditions. Fig. 5 displays the SEM images obtained under two experimental

conditions. A significant decrease of AgNPs size was reached by decreasing the deposition charge, being smaller at higher overpotentials. Thus, applying a potential of +0.10 V and deposition charge of 1.5 mC higher polydispersity was obtained than applying a more negative potential of -0.025 V and a lower deposition charge of 1.2 mC, where the medium size of AgNPs was 28 ± 4 nm.

According to these results, the most convenient potential range to perform potentiostatic deposition of AgNPs, in order to obtain more monodispersity and homogeneous distribution of AgNPs from BmpyrNTf$_2$ solution, corresponds to the final part of C$_1$ peak, i.e., around 0.00 V. Applying these potentials and being the deposition charge involved low, the electrodeposition of small and monodisperse AgNPs can be achieved, tailored them only by controlling the charge involved in the formation process.

3.3. AgNPs electrodeposition on FS-SWCNT electrodes.

One of the main highlights of the FS-SWCNT electrodes is related to the capability of these SWCNT films to be modified, creating, as in this work, Janus nanostructures. Fig. S1d in Supporting Information shows a scheme of the Janus nanostructure developed in this section. As can be seen in the scheme, the main objective of this work is the functionalization of only one side of the FS-SWCNT membrane with AgNPs, keeping unmodified the other side of the SWCNT electrode. Once demonstrated section 3.2 that the electrodeposition of AgNPs on SWCNT electrodes from BmpyrNTf$_2$ solution was achieved, the electrochemical functionalization of FS-SWCNT with AgNPs was studied by spectroelectrochemistry. The good conductivity and good transparency to UV-Vis radiation exhibited by FS-SWCNT electrodes makes them suitable electrodes for monitoring their functionalization by UV-Vis absorption

spectroelectrochemistry. At this point, the electrodeposition of AgNPs was carried out in 8×10^{-3} M $AgNO_3$ in $BmpyrNTf_2$ at room temperature using a FS-SWCNT membrane as working electrode. Taking into account that both, SWCNT and FS-SWCNT electrodes, were fabricated using the same SWCNT dispersion, a similar electrochemical behaviour was expected by both types of electrodes. Therefore, the same electrochemical conditions used with SWCNT electrodes were used to work with the FS-SWCNT electrodes, i.e, overpotentials around 0.00 V and low deposition charges were selected to perform their functionalization with AgNPs. Spectroelectrochemical studies allow us to record simultaneously both electrochemical and spectroscopic responses and, in this way, to monitor the formation of AgNPs on one side of the FS-SWCNT electrode.

Fig. 6a and Fig. 6b display the UV-Vis spectra recorded in transmission configuration [59] during the electrodeposition of AgNPs at fixed charge of 1.5 mC applying -0.025 V and +0.05 V, respectively. UV-Vis spectra show only one absorption band emerging and increasing during the electrodeposition process that corresponds to the plasmon band of AgNPs generated. The plasmon band of the two experiments performed at two different overpotentials, increases concomitantly with the charge involved (Fig. 7). However, an accurate analysis of the evolution and waveform of the two plasmon bands denotes some significant differences that should be linked with the reaction mechanism and the final characteristics of the AgNPs electrogenerated. The first differences are related to the waveform of the final absorption spectra of the NPs deposited on the FS-SWCNT electrode. The plasmon band is centred at 450 nm with a half-band width equal to 278 nm when the potential applied is -0.025 V (Fig. 6a), while at +0.05 V the plasmon band peaks at 430 nm and the half-band width is 306 nm (Fig. 6b). Additionally, analyzing the ratio between the absorbance at the maximum of the plasmon band (A_{max}) and the

absorbance at 800 nm (A_{800nm}, the tail of the absorption band), A_{max}/A_{800nm}, has a value of 7.62 when the potential applied is -0.025 V and 3.30 when it is +0.05 V. These results point out that at higher overpotentials (-0.025 V) narrower and more symmetric plasmon band is recorded, leading to less polydisperse AgNPs and a homogeneous deposition on the FS-SWCNT electrode. The medium size of AgNPs, determined from SEM images (Fig. S7 in Supporting Information), at -0.025 V was 38 ± 2 nm. It is noteworthy that the maximum of absorbance reached at -0.025 V is approximately 25% higher than at +0.05, indicating that the deposition charge has been used more efficiently in the generation of smaller and more monodisperse NPs as the SEM images obtained under similar conditions on SWCNTs shown in Fig. 5.

Analyzing now the relationship between the deposition charge and the absorbance at the maximum of the plasmon band, 450 and 430 nm, (Fig. 7) it can be appreciated, in both cases, a concomitant increase of absorbance values with the decrease of the deposition charge. A more in depth study reveals some differences that can explain the different characteristics observed in the AgNPs electrodeposited on the FS-SWCNT electrode. At -0.025 V, two different slopes are observed, the first linear increase of absorbance at 450 nm takes place until 170 s (Fig. 7a), with a slope of 5.66×10^{-4} s^{-1}, being more pronounced than the increase of the absorbance at 430 nm, illustrated in Fig. 7b, related to the experiment performed at +0.05 V. During the last 300 s at -0.025 V, the slope of the chronoabsorptogram at 450 nm diminished to 1.95×10^{-4} s^{-1}. This behavior denotes that a kinetic of the reduction of Ag(I) to AgNPs faster in the first 170 s than in the next 300 s leads to more monodisperse quasi-spherical AgNPs. However, at +0.05 V absorbance at 430 nm increases linearly 150 s onwards, with a slope of 4.00×10^{-4} s^{-1}, indicating that a high kinetic constant during the second part of the synthesis leads to more polydisperse nanoparticles. SEM images taken from the Janus FS-SWCNT electrode side where AgNPs were

17

electrodeposited (Fig. S7 in Supporting Information) agree with the spectroelectrochemical results. Fig. S7a in Supporting Information shows that the electrodeposition at -0.025 V leads to a homogeneous deposition of more monodisperse AgNPs on the FS-SWCNT membrane than at +0.05 V where the polydispersity is significantly higher. Furthermore, the distribution of AgNPs on the SWCNT film is independent on the potential applied (-0.025 V or +0.05 V) and not specific distribution of AgNPs is observed in SEM images (Fig. S7 in Supporting Information).

EDX analysis of the two faces of the FS-SWCNT membranes, side A and B in the scheme shown in Fig. S1d in Supporting Information, is presented in Fig. S8 in Supporting Information. These EDX images show that only the face in contact with Ag(I) solution is functionalized with AgNPs (side A), as is evidenced by the Ag peak appreciated around 3 keV. However, the other face (side B) remains unmodified; the main peaks observed are related to C and O from the SWCNT film, and Al and Si probably related to the presence of dust deposited during the fabrication and/or functionalization processes. Therefore, according to the results presented in this work and taking as reference a previous work [50], it can be concluded that only one face of the FS-SWCNT electrode has been independently functionalized with AgNPs without interference between both faces, fact that opens new gates for simple design of Janus materials.

4. Conclusions

The development of new strategies in the functionalization of different materials with the final objective of obtaining Janus structures is necessary because these hybrid materials are one of the most interesting systems for very attractive applications. Although the design of these materials depends on the final properties required, sometimes the methodology employed on the modification of raw materials is not as easy and clean as would be desired. In the present study,

the independent functionalization of one face of FS-SWCNT film has been established, being this study a first step in the design of more complex Janus materials using these SWCNT membranes. The use of ionic liquid as solvent and electrolytic medium not only involves a green procedure in the electrodeposition of AgNPs, but it will also allow the simultaneous electrochemical functionalization of the both faces of FS-SWCNT electrodes in future works, one with AgNPs in ionic liquid and the backside with less noble metallic NPs using aqueous medium.

In a first step, AgNPs electrodeposition from $BmpyrNTf_2$ solution has been performed in different carbon substrates, such as GC and SWCNTs, to optimize the electrodeposition conditions using low Ag(I) concentrations. This optimization step, where the most suitable experimental conditions were stablished, has led to conclude that high overpotentials involve a lower efficiency in the Ag(I) reduction, due to the simultaneous reduction of the ionic liquid. The delay detected in the reduction of Ag(I) in $BmpyrNTf_2$ solution using SWCNT films as electrodes when compared with its reduction on GC surfaces, is related to the lower conductivity of the 2D configuration of the SWCNT electrodes prepared that promotes the appearance of silver electrodeposition at less positive potentials.

In the last step, the fabrication of Janus membranes has been carried out by functionalization of only one of the two faces of FS-SWCNT films, studying the process with UV-Vis absorption spectroelectrochemistry, and with the specific modification being confirmed by SEM and EDX analysis. Small and more monodisperse AgNPs have been electrodeposited on the FS-SWCNT membranes when relative high overpotentials and low deposition charges were applied. SEM images and UV-Vis absorption spectroelectrochemistry has been determinant to discriminate the

generation of different kind of AgNPs on the FS-SWCNT electrodes and to establish the kinetic of electrodeposition of these AgNPs, at different overpotentials.

This work opens new gates for future modifications of free-standing conductive membranes, becoming the design of Janus structures more customizable to the required needs.

Appendix A. Supplementary data.

Supplementary information associated with this article can be found in the online version.

Acknowledgement

References

[1]   X. Ji, Q. Zhang, F. Liang, Q. Chen, X. Qu, C. Zhang, Q. Wang, J. Li, X. Song, Z. Yang, Ionic liquid functionalized Janus nanosheets, Chem. Commun. 50 (2014) 5706–5709.

[2]   S. Fujii, M. Kappl, H.-J. Butt, T. Sugimoto, Y. Nakamura, Soft Janus Colloidal Crystal Film, Angew. Chemie Int. Ed. 51 (2012) 9809–9813.

[3]   E. Shaviv, O. Schubert, M. Alves-Santos, G. Goldoni, R. Di Felice, F. Vallée, N. Del Fatti, U. Banin, C. Sönnichsen, Absorption Properties of Metal-Semiconductor Hybrid Nanoparticles, ACS Nano. 5 (2011) 4712–4719.

[4]   H. Liang, A. Cacciuto, E. Luijter, S. Granick, Clusters of charged janus spheres, Nano Lett. 6 (2006) 2510–2514.

[5]   S. Chen, S.-Z. Qiao, Hierarchically Porous Nitrogen-Doped Graphene–NiCo$_2$O$_4$ Hybrid Paper as an Advanced Electrocatalytic Water-Splitting Material, ACS Nano. 7 (2013) 10190–10196.

[6]   A. Walther, A.H.E. Müller, Janus particles: synthesis, self-assembly, physical properties, and applications., Chem. Rev. 113 (2013) 5194–261.

[7]   X. Pang, C. Wan, M. Wang, Z. Lin, Strictly Biphasic Soft and Hard Janus Structures: Synthesis, Properties, and Applications, Angew. Chemie Int. Ed. 53 (2014) 5524–5538.

[8]   L. Hu, G. Gruner, D. Li, R.B. Kaner, J. Cech, Patternable transparent carbon nanotube films for electrochromic devices, J. Appl. Phys. 101 (2007) 016102.

[9]   R. Malavé Osuna, V. Hernández, J.T. López Navarrete, E.I. Kauppinen, V. Ruiz, Ultrafast and High-Contrast Electrochromism on Bendable Transparent Carbon Nanotube Electrodes, J. Phys. Chem. Lett. 1 (2010) 1367–1371.

[10]   P. Yáñez-Sedeño, J.M. Pingarrón, J. Riu, F.X. Rius, Electrochemical sensing based on carbon nanotubes, TrAC - Trends Anal. Chem. Trends Anal. Chem. 29 (2010) 939–953.

[11]   M. Trojanowicz, Analytical applications of carbon nanotubes: a review, TrAC - Trends Anal. Chem. 25 (2006) 480–489.

[12]   F. Liu, Y. Piao, K.S. Choi, T.S. Seo, Fabrication of free-standing graphene composite films as electrochemical biosensors, Carbon 50 (2012) 123–133.

[13]   A.G. Nasibulin, A. Kaskela, K. Mustonen, A.S. Anisimov, V. Ruiz, S. Kivistö, S. Rackauskas, M.Y. Timmermans, M. Pudas, B. Aitchison, M. Kauppinen, D.P. Brown, O.G. Okhotnikov, E.I. Kauppinen, Multifunctional Free-Standing Single-Walled Carbon Nanotube Films, ACS Nano. 5 (2011) 3214–3221.

[14]   Z. Niu, W. Zhou, J. Chen, G. Feng, H. Li, W. Ma, J. Li, H. Dong, Y. Ren, D. Zhao, S. Xie, Compact-designed supercapacitors using free-standing single-walled carbon nanotube films, Energy Environ. Sci. 4 (2011) 1440–1446.

[15] B.J. Mason, S. Chang, J. Chen, S.B. Cronin, A.W. Bushmaker, Thermoacoustic Transduction in Individual Suspended Carbon Nanotubes, ACS Nano. 9 (2015) 5372–5376.

[16] L. Noerochim, J.-Z. Wang, S.-L. Chou, D. Wexler, H.-K. Liu, Free-standing single-walled carbon nanotube/SnO_2 anode paper for flexible lithium-ion batteries, Carbon 50 (2012) 1289–1297.

[17] S.Y. Chew, S.H. Ng, J. Wang, P. Novák, F. Krumeich, S.L. Chou, J. Chen, H.K. Liu, Flexible free-standing carbon nanotube films for model lithium-ion batteries, Carbon 47 (2009) 2976–2983.

[18] C. Casagrande, P. Fabre, E. Raphael, M. Veyssie, "Janus Beads": Realization and Behaviour at Water/Oil Interfaces., Eur. Lett. 9 (1989) 251–255.

[19] J. Hu, S. Zhou, Y. Sun, X. Fang, L. Wu, Fabrication, properties and applications of Janus particles., Chem. Soc. Rev. 41 (2012) 4356–4378.

[20] W. Zhang, G. Wang, Research and development for antibacterial materials of silver nanoparticle, New Chem Mater. 31 (2003) 42–44.

[21] J. Zhu, S. Liu, O. Palchik, Y. Koltypin, A. Gedanken, Shape-controlled synthesis of silver nanoparticles by pulse sonoelectrochemical methods, Langmuir. 16 (2000) 6396–6399.

[22] N. Horimoto, N. Ishikawa, A. Nakajima, Preparation of a SERS substrate using vacuum-synthesized silver nanoparticles, Chem. Phys. Lett. 413 (2005) 78–83.

[23] D. Ibañez, C. Fernandez-Blanco, A. Heras, A. Colina, Time-resolved study of the surface-enhanced Raman scattering effect of silver nanoparticles generated in voltammetry experiments., J. Phys. Chem. C. 118 (2014) 23426–23433.

[24] Y. Liu, K. Yang, T. Hsu, Improved Surface-Enhanced Raman Scattering Performances on Silver−Silica Nanocomposites, J. Phys. Chem. C. 113 (2009) 8162–8168.

[25] G.M. Zarkadas, A. Stergiou, G. Papanastasiou, Influence of citric acid on the silver electrodeposition from aqueous $AgNO_3$ solutions, Electrochim. Acta. 50 (2005) 5022–5031.

[26] A. Milchev, E. Vassileva, V. Kertov, Electrolytic nucleation of silver on a glassy carbon electrode. Part I. Mechanism of critical nucleus formation, J. Electroanal. Chem. 107 (1980) 323–336.

[27] A. Milchev, E. Vassileva, Electrolytic nucleation of silver on a glassy carbon electrode. Part II. Steady-state nucleation rate, J. Electroanal. Chem. 107 (1980) 337–352.

[28] A. Milchev, B. Scharifker, G. Hills, A potentiostatic study of the electrochemical nucleation of silver on vitreous carbon, J. Electroanal. Chem. 132 (1982) 277–289.

[29] E. Michailova, A. Milchev, Influence of potassium sodium tartrate on the initial stage of silver electrodeposition, J. Appl. Electrochem. 21 (1991) 170–174.

[30] G. Sandmann, H. Dietz, W. Plieth, Preparation of silver nanoparticles on ITO surfaces by a double-pulse method, J. Electroanal. Chem. 491 (2000) 78–86.

[31] M. Palomar-Pardavé, M.T. Ramírez, I. González, A. Serruya, B.R. Scharifker, Silver electrocrystallization on vitreous carbon from ammonium hydroxide solutions, J. Electrochem. Soc. 143 (1996) 1551–1558.

[32] E. Gómez, J. García-Torres, E. Vallés, Study and preparation of silver electrodeposits at negative potentials, J. Electroanal. Chem. 594 (2006) 89–95.

[33] E. Gómez, J. García-Torres, E. Vallés, Electrodeposition of silver as a precursor matrix of magnetoresistive materials, Mater. Lett. 61 (2007) 1671–1674.

[34] G.M. De Oliveira, L.L. Barbosa, R.L. Broggi, I.A. Carlos, Voltammetric study of the influence of EDTA on the silver electrodeposition and morphological and structural characterization of silver films, J. Electroanal. Chem. 578 (2005) 151–158.

[35] J. Ustarroz, U. Gupta, A. Hubin, S. Bals, H. Terryn, Electrodeposition of Ag nanoparticles onto carbon coated TEM grids: A direct approach to study early stages of nucleation, Electrochem. Commun. 12 (2010) 1706–1709.

[36] A. Florea, A. Petică, L. Anicăi, T. Visan, Preliminary studies of silver coatings formation from choline chloride based ionic liquids, UPB Sci. Bull. Ser. B Chem. Mater. Sci. 72 (2010) 115–126.

[37] P. Sebastián, E. Vallés, E. Gómez, First stages of silver electrodeposition in a deep eutectic solvent. Comparative behavior in aqueous medium, Electrochim. Acta. 112 (2013) 149–158.

[38] A.P. Abbott, K.E. Ttaib, G. Frisch, K.S. Ryder, D. Weston, The electrodeposition of silver composites using deep eutectic solvents, Phys. Chem. Chem. Phys. 14 (2012) 2443–2449.

[39] F. Endres, W. Freyland, Electrochemical scanning tunneling microscopy investigation of HOPG and silver electrodeposition on HOPG from the acid room-temperature molten salt aluminum chloride-1-methyl-3-butyl-imidazolium chloride, J. Phys. Chem. B. 102 (1998) 10229–10233.

[40] C.A. Zell, F. Endres, W. Freyland, Electrochemical in situ STM study of phase formation during Ag and Al electrodeposition on Au(111) from a room temperature molten salt, Phys. Chem. Chem. Phys. 1 (1999) 697–704.

[41] P. He, H. Liu, Z. Li, Y. Liu, X. Xu, J. Li, Electrochemical deposition of silver in room-temperature ionic liquids and its surface-enhanced Raman scattering effect, Langmuir. 20 (2004) 10260–10267.

[42] T.-H. Tsai, S. Thiagarajan, S.-M. Chen, Green synthesis of silver nanoparticles using ionic liquid and application for the detection of dissolved oxygen, Electroanalysis. 22 (2010) 680–687.

[43] A. Basile, A.I. Bhatt, A.P. O'Mullane, S.K. Bhargava, An investigation of silver

electrodeposition from ionic liquids: Influence of atmospheric water uptake on the silver electrodeposition mechanism and film morphology, Electrochim. Acta. 56 (2011) 2895–2905.

[44] R. Fukui, Y. Katayama, T. Miura, The influence of potential on electrodeposition of silver and formation of silver nanoparticles in some ionic liquids, J. Electrochem. Soc. 158 (2011) D567–D572.

[45] A. Ispas, M. Pölleth, K.H.T. Ba, A. Bund, J. Janek, Electrochemical deposition of silver from 1-ethyl-3-methylimidazolium trifluoromethanesulfonate, Electrochim. Acta. 56 (2011) 10332–10339.

[46] S. Zein El Abedin, F. Endres, Electrodeposition of nanocrystalline silver films and nanowires from the ionic liquid 1-ethyl-3-methylimidazolium trifluoromethylsulfonate, Electrochim. Acta. 54 (2009) 5673–5677.

[47] R. Bomparola, S. Caporali, A. Lavacchi, U. Bardi, Silver electrodeposition from air and water-stable ionic liquid: An environmentally friendly alternative to cyanide baths, Surf. Coatings Technol. 201 (2007) 9485–9490.

[48] B.H.R. Suryanto, C.A. Gunawan, X. Lu, C. Zhao, Tuning the electrodeposition parameters of silver to yield micro/nano structures from room temperature protic ionic liquids, Electrochim. Acta. 81 (2012) 98–105.

[49] F.A.A. Figueredo-Sobrinho, L.P.M. Santos, D.S. Leite, D.C. Craveiro, S.H. Santos, K.I.B. Eguiluz, G.R. Salazar-Banda, C.D. Maciel, M.D. Coutinho-Neto, P. Homem-De-Mello, P. De Lima-Neto, A.N. Correia, Morphological dependence of silver electrodeposits investigated by changing the ionic liquid solvent and the deposition parameters, Phys. Chem. Chem. Phys. 18 (2016) 7242–7250.

[50] D. Ibañez, J. Garoz-Ruiz, D. Plana, A. Heras, D.J. Fermín, A. Colina, Spectroelectrochemistry at free-standing carbon nanotubes electrodes, Electrochim. Acta. 217 (2016) 262–268.

[51] D. Ibañez, J. Garoz-Ruiz, A. Heras, A. Colina, Simultaneous UV–Visible Absorption and Raman Spectroelectrochemistry, Anal. Chem. 88 (2016) 8210–8217.

[52] D. Ibañez, E.C. Romero, A. Heras, A. Colina, Dynamic Raman Spectroelectrochemistry of Single Walled Carbon Nanotubes modified electrodes using a Langmuir-Schaefer method, Electrochim. Acta. 129 (2014) 171–176.

[53] D. Ibañez, A. Santidrian, A. Heras, M. Kalbáč, A. Colina, Study of adenine and guanine oxidation mechanism by surface-enhanced Raman spectroelectrochemistry, J. Phys. Chem. C. 119 (2015) 8191–8198.

[54] N. González-Diéguez, A. Colina, J. López-Palacios, A. Heras, Spectroelectrochemistry at screen-printed electrodes: Determination of dopamine, Anal. Chem. 84 (2012) 9146–9153.

[55] C. Fernandez-Blanco, D. Ibañez, A. Colina, V. Ruiz, A. Heras, Spectroelectrochemical

study of the electrosynthesis of Pt nanoparticles/poly(3,4-(ethylenedioxythiophene) composite, Electrochim. Acta. 145 (2014) 139–147.

[56]   L. Kavan, L. Dunsch, Spectroelectrochemistry of Carbon Nanostructures, ChemPhysChem. 8 (2007) 974–998.

[57]   J. Garoz-Ruiz, D. Izquierdo, A. Colina, S. Palmero, A. Heras, Optical fiber spectroelectrochemical device for detection of catechol at press-transferred single-walled carbon nanotubes electrodes., Anal. Bioanal. Chem. 405 (2013) 3593–3602.

[58]   J. Garoz-Ruiz, S. Palmero, D. Ibañez, A. Heras, A. Colina, Press-transfer optically transparent electrodes fabricated from commercial single-walled carbon nanotubes, Electrochem. Commun. 25 (2012) 1–4.

[59]   J. Garoz-Ruiz, A. Heras, S. Palmero, A. Colina, Development of a Novel Bidimensional Spectroelectrochemistry Cell Using Transfer Single-Walled Carbon Nanotubes Films as Optically Transparent Electrodes., Anal. Chem. 87 (2015) 6233–6239.

[60]   G. Gunawardena, G. Hills, I. Montenegro, B. Scharifker, Electrochemical nucleation. Part I. General considerations, J. Electroanal. Chem. 138 (1982) 225–239.

[61]   B. Scharifker, G. Hills, Theoretical and experimental studies of multiple nucleation, Electrochim. Acta. 28 (1983) 879–889.

[62]   L.M.C. Pinto, E. Spohr, P. Quaino, E. Santos, W. Schmickler, Why silver deposition is so fast: Solving the enigma of metal deposition, Angew. Chemie - Int. Ed. 52 (2013) 7883–7885.
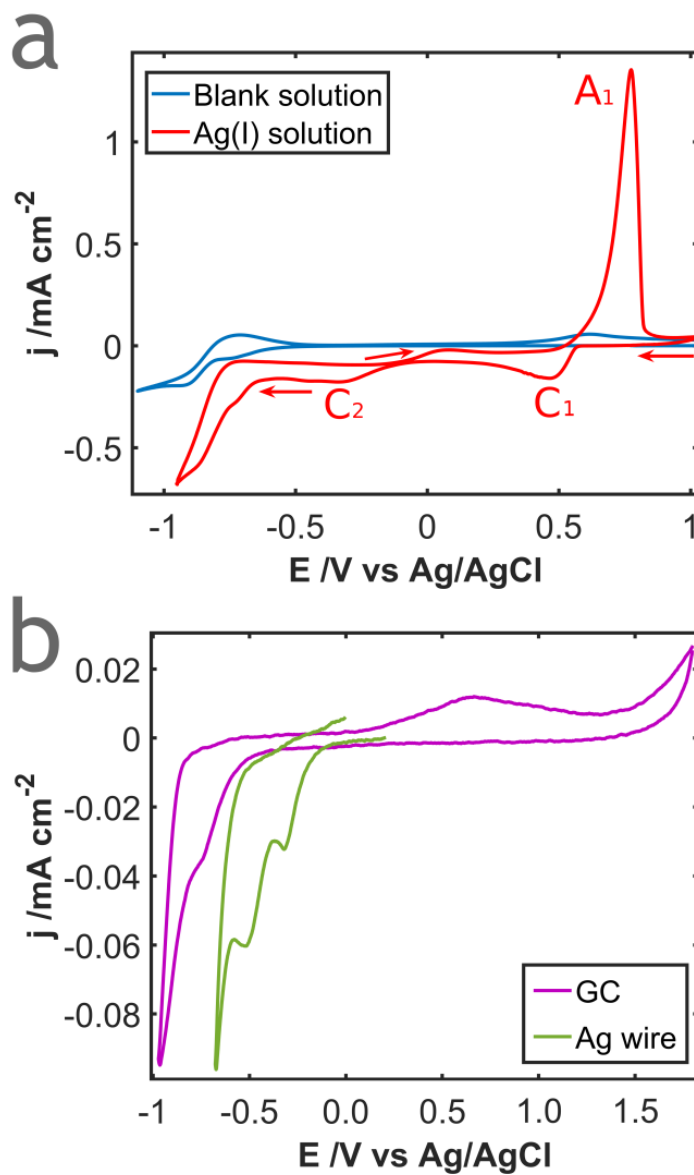
Figures

Figure 1

Figure 1. (a) Cyclic voltammograms obtained in BmpyrNTf$_2$ (blue line) and of 8×10^{-3} M AgNO$_3$ in BmpyrNTf$_2$ (red line) using a GC electrode. (b) Cyclic voltammograms obtained in BmpyrNTf$_2$ using a GC electrode (purple line) and a small Ag ball (green line) as a working electrode. Scan rate 0.010 V s^{-1}
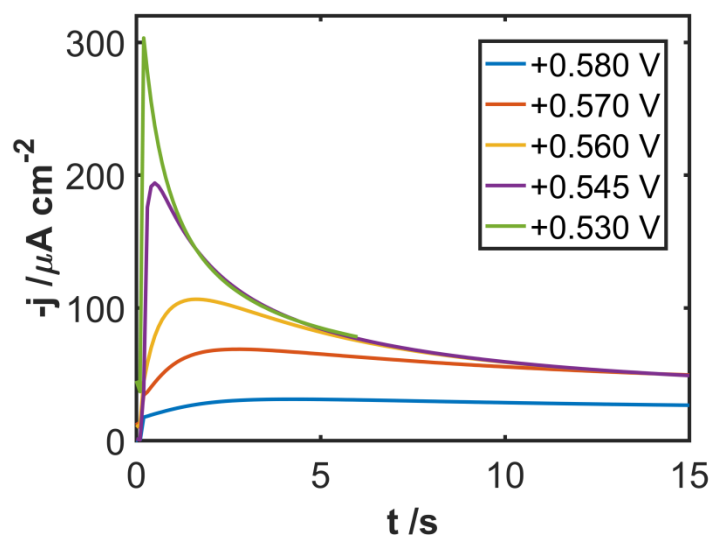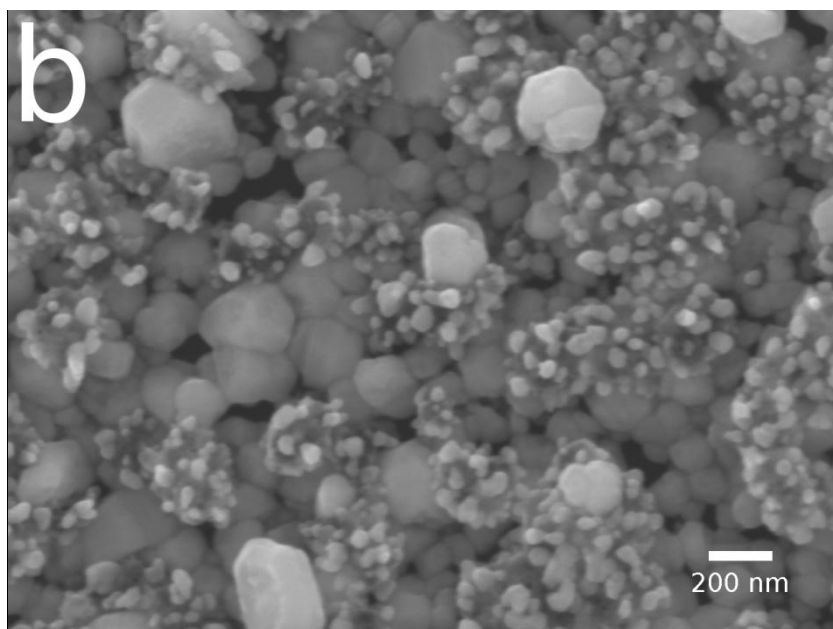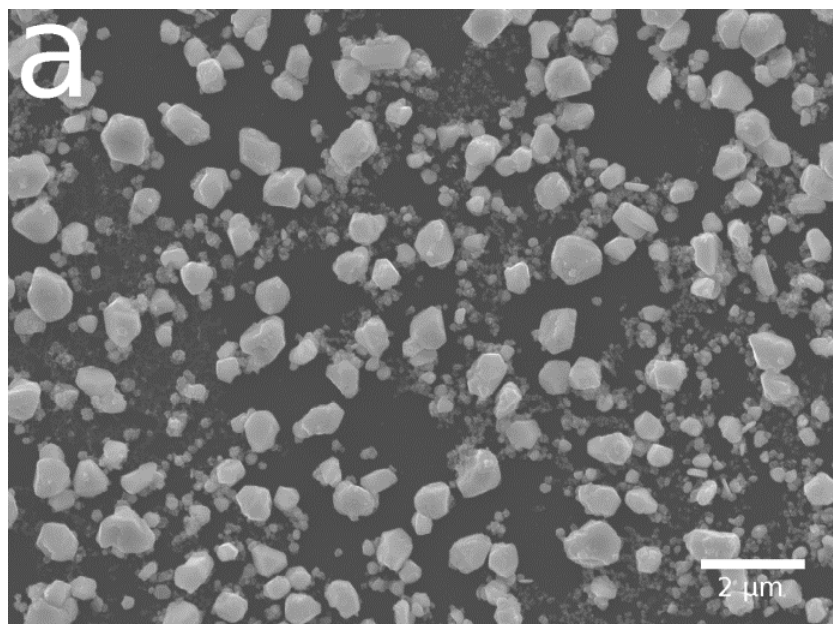
26

Figure 2

Figure 2. Potentiostatic curves (j *vs* time) of 8×10^{-3} M AgNO$_3$ in BmpyrNTf$_2$, obtained at +0.580 V (blue line), +0.570 V (orange line), +0.560 V (yellow line), +0.545 V (purple line) and +0.530 V (green line) using a GC electrode.

Figure 3
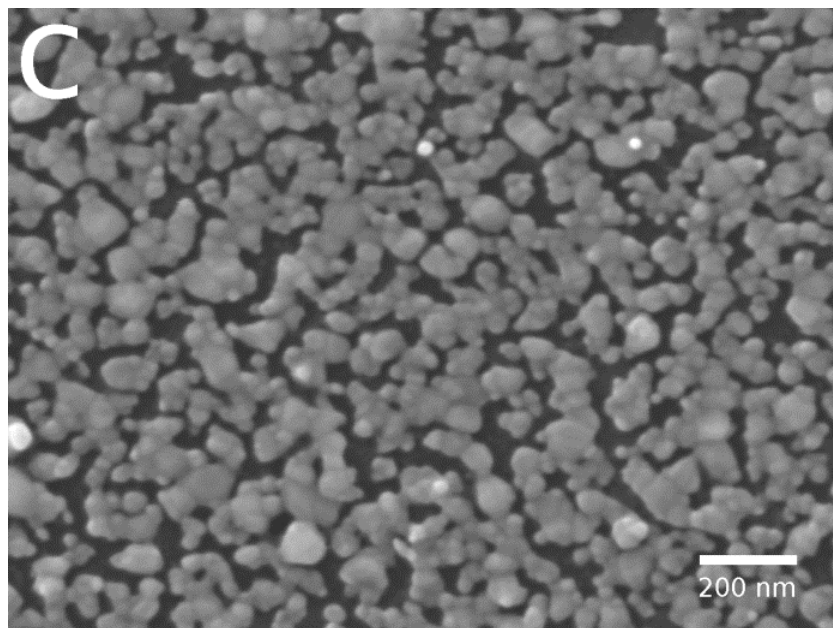
Figure 3. SEM images of Ag electrodeposition from 8×10^{-3} M AgNO$_3$ in BmpyrNTf$_2$ on GC electrode at different potentials: (a) +0.56 V, (b) +0.16 V and (c) -0.60 V, and fixing the deposition charge to 8 mC.

Figure 4
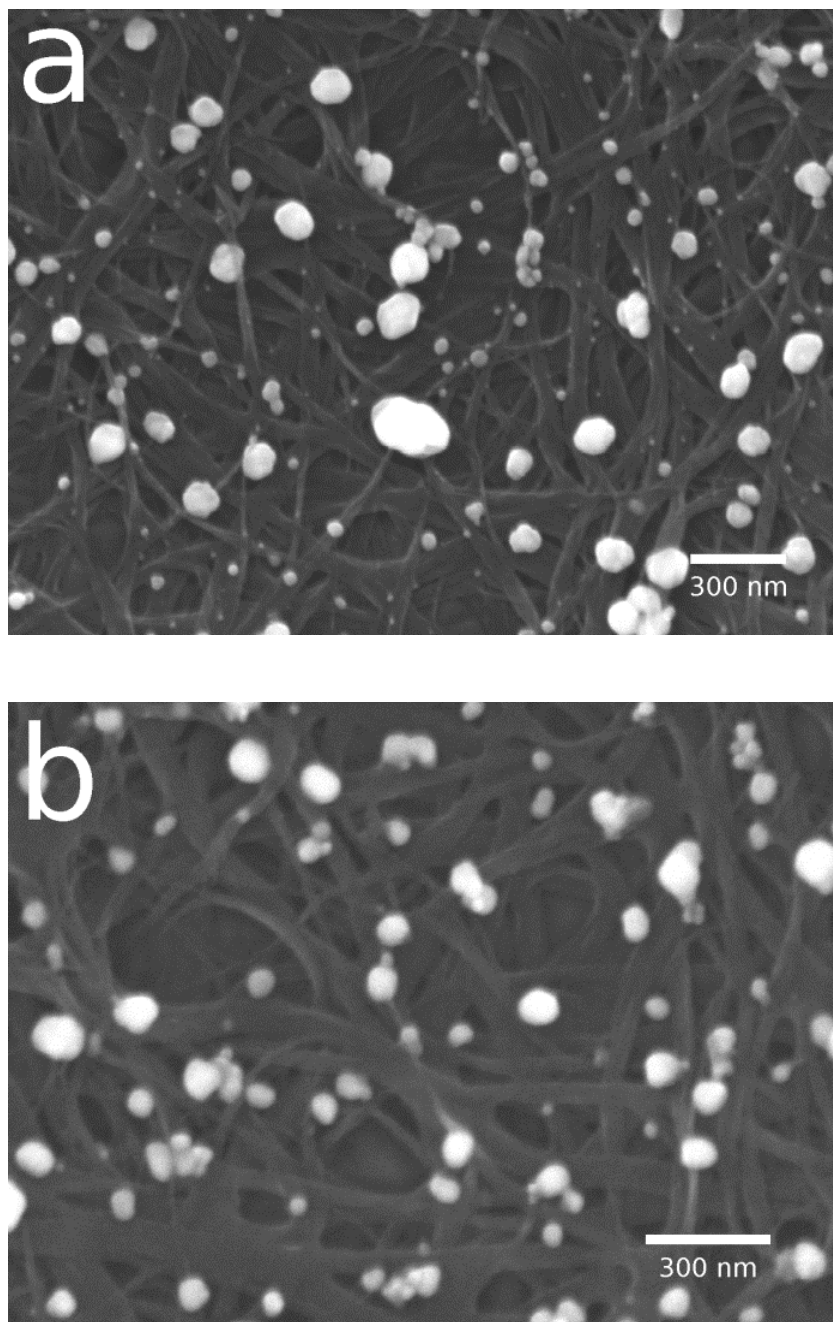
Figure 4. SEM images of AgNPs electrogenerated from 8×10^{-3} M AgNO$_3$ in BmpyrNTf$_2$ on SWCNT electrode at different potentials: (a) +0.05 V and (b) 0.00 V, and fixing the deposition charge to 6 mC.
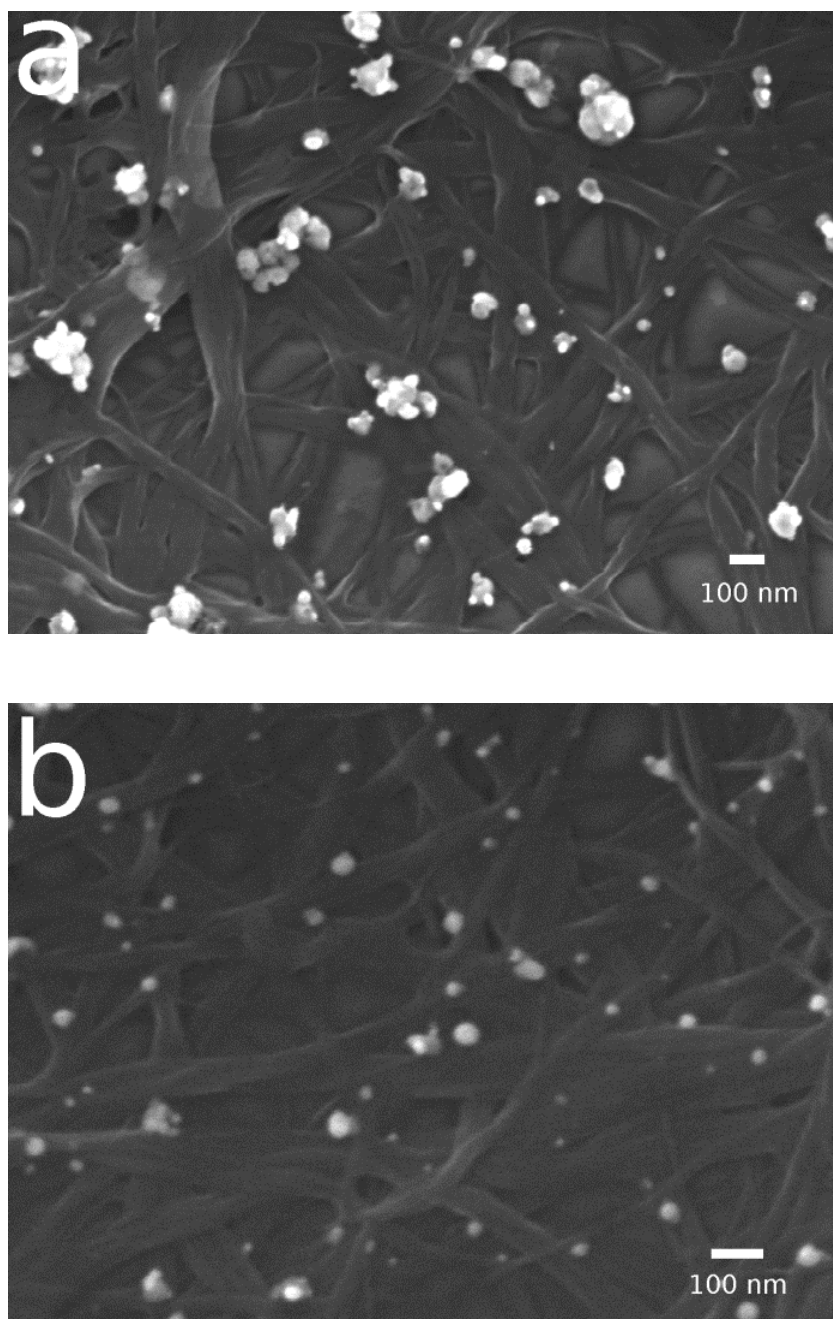
Figure 5

Figure 5. SEM images of AgNPs electrogenerated from 8×10^{-3} M AgNO$_3$ in BmpyrNTf$_2$ on SWCNT electrode at different potentials and deposition charges: (a) +0.10 V and 1.5 mC, and (b) -0.025 V and 1.2 mC.
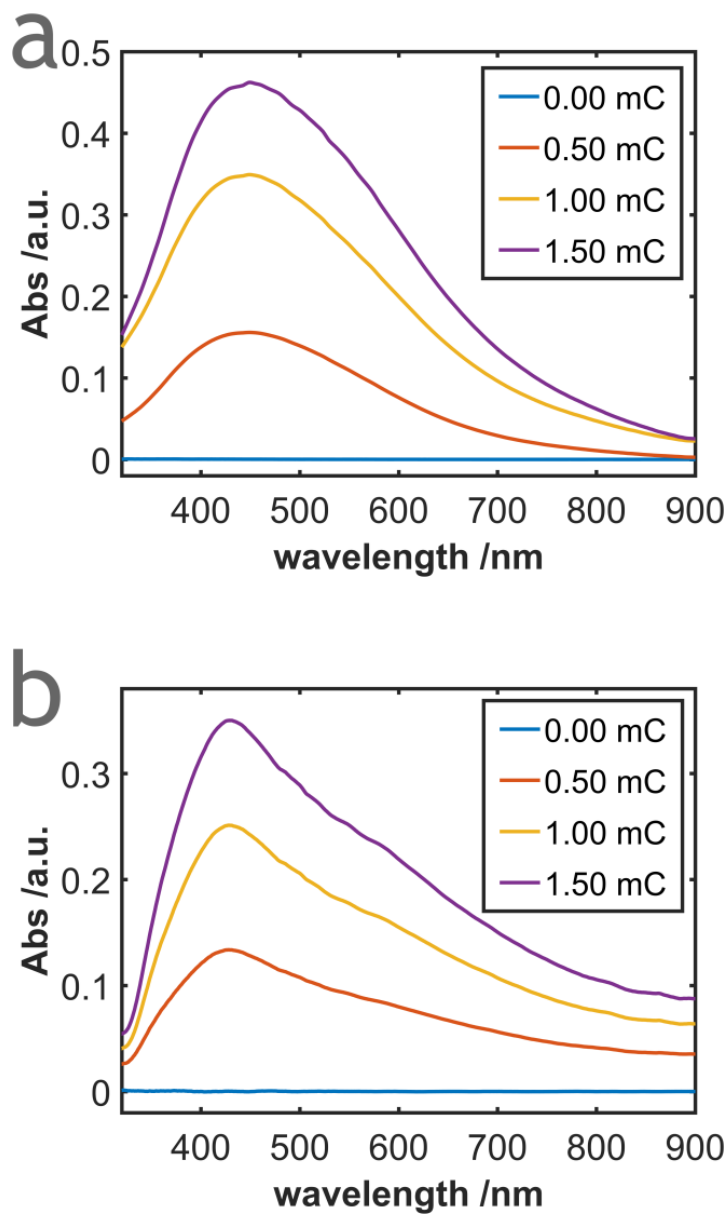
Figure 6

Figure 6. Evolution of UV-Vis spectra recorded during the potentiostatic deposition of AgNPs from 8×10^{-3} M AgNO$_3$ in BmpyrNTf$_2$ on FS-SWCNT electrodes applying (a) -0.025 V and (b) +0.05 V and fixing the deposition charge to 1.5 mC.
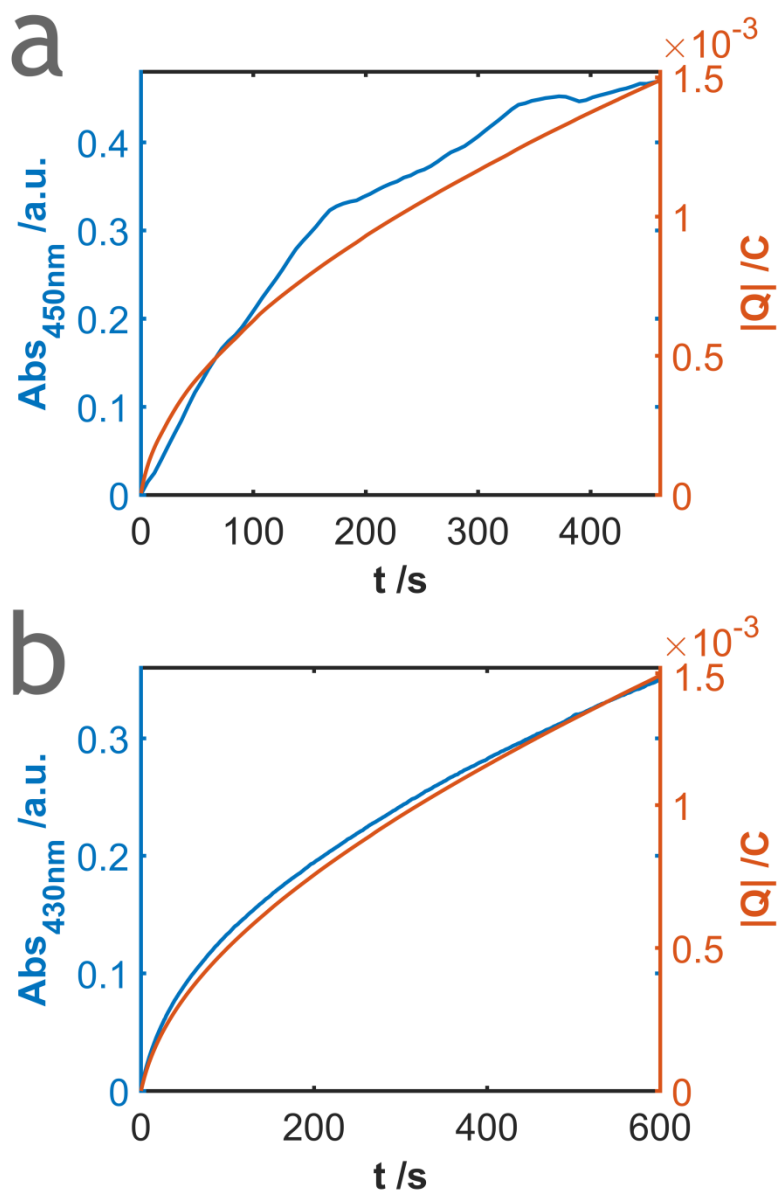
Figure 7

Figure 7. Comparison of the evolution of the absorbance of the UV-Vis plasmon band (blue lines) and the evolution of the charge involved (brown lines) in the electrodeposition of AgNPs from 8×10^{-3} M AgNO$_3$ in BmpyrNTf$_2$ on FS-SWCNT electrodes at (a) -0.025 V and (b) +0.05 V and fixing the deposition charge to 1.5 mC.

Graphical abstract